

60th Anniversary Issue: Biological

Electron crystallography for structural and functional studies of membrane proteins

Yoshinori Fujiyoshi*

Structural Physiology, Department of Biophysics, Graduate School of Science, Kyoto University, Oiwake, Kitashirakawa, Sakyo-ku, Kyoto 606-8502, Japan

*To whom correspondence should be addressed. E-mail: yoshi@em.biophys.kyoto-u.ac.jp

Abstract

Membrane proteins are important research targets for basic biological sciences and drug design, but studies of their structure and function are considered difficult to perform. Studies of membrane structures have been greatly facilitated by technological and instrumental advancements in electron microscopy together with methodological advancements in biology. Electron crystallography is especially useful in studying the structure and function of membrane proteins. Electron crystallography is now an established method of analyzing the structures of membrane proteins in lipid bilayers, which resembles their natural biological environment. To better understand the neural system function from a structural point of view, we developed the cryo-electron microscope with a helium-cooled specimen stage, which allows for analysis of the structures of membrane proteins at a resolution higher than 3 Å. This review introduces recent instrumental advances in cryo-electron microscopy and presents some examples of structure analyses of membrane proteins, such as bacteriorhodopsin, water channels and gap junction channels. This review has two objectives: first, to provide a personal historical background to describe how we came to develop the cryo-electron microscope and second, to discuss some of the technology required for the structural analysis of membrane proteins based on cryo-electron microscopy.

Keywords

electron crystallography, high-resolution electron microscopy, cryo-electron microscope, liquid helium-cooled specimen stage, channels, membrane proteins

Received

4 March 2011, accepted 16 April 2011

Introduction

There are many interesting questions in brain science that are very difficult to answer. For example, how do education and other experiences in human development influence cognitive ability and personality in the adult? The molecular mechanisms underlying such phenomena are completely unknown. Understanding these brain functions and other biological functions requires a more complete understanding of ion channels. Therefore, for

example, studies of the structure and function of bacterial and mammalian Na⁺ channels, which are very important voltage-gated cation channels, remain a challenge. Single-particle analysis using cryo-electron microscopy (cryo-EM) revealed the complex structure of the voltage-sensitive Na⁺ channel purified from the electric organ of the electric eel [1]. For supporting ion channel functions in brain, water channels are also important because the water content of the brain is, remarkably, as

much as 85%, and even when water molecules rapidly pass through the water channels, ion permeation must be blocked to ensure ion channel function.

Electron crystallography is a particularly useful method for structure analyses of membrane proteins such as ion channels and water channels, for the following reasons:

- (1) Structures can be analyzed in membranes that provide an environment similar to the native conditions of the protein.
- (2) Structures can be analyzed even when only poor-quality crystals are available, although resolution is strongly related to crystal quality.
- (3) Both sides of the specimen are kept open and there is less influence from artificial crystal packing, as described later for the structure analysis of the gap junction channel. Furthermore, this feature enables researchers to use the freeze-trapping technique, which

was developed and used to study the gating mechanism of a nicotinic acetylcholine receptor by Unwin [2].

- (4) Phases for structure analysis are calculated directly from images and provide a better quality map than does X-ray crystallography at the same resolution.

Electron crystallography was the first method used to obtain a real image of the membrane protein bacteriorhodopsin, whose structure was analyzed by Henderson and Unwin in 1975 [3]. This method is extremely powerful, especially for structural studies of membrane proteins. Henderson *et al.* [4] were the first to use it to determine the atomic structure of bacteriorhodopsin based on electron crystallography. The adoption of this method in structural biology has been slow, presumably due to technological difficulties. Electron crystallography should be the core method for performing structural and functional studies of

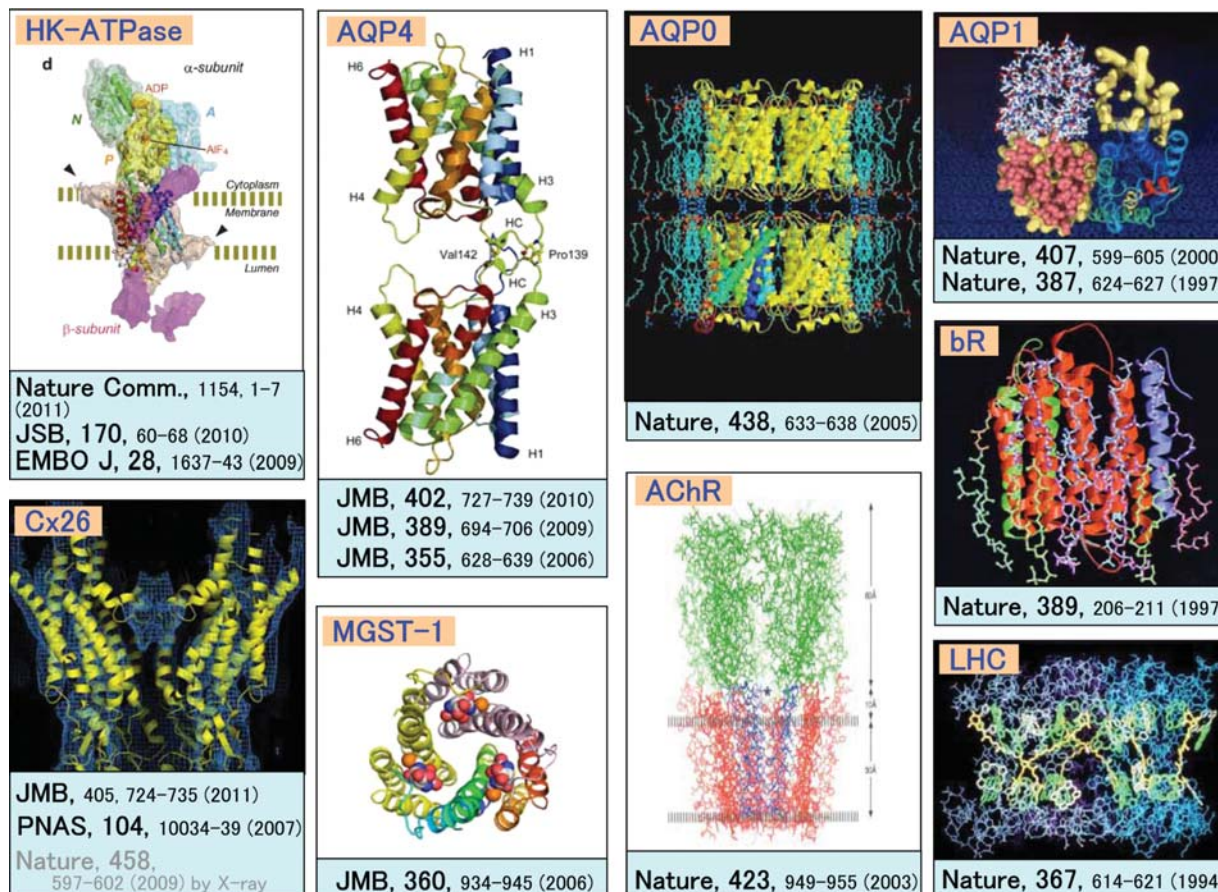


Fig. 1. Structures of membrane proteins analyzed using the originally developed cryo-EM systems.

membrane proteins (see Fig. 1 for examples of analyses that have been performed using this method).

High-resolution EM

High-resolution structure analysis by electron crystallography requires image data at high resolution, preferably atomic-level resolution. Whether EM could provide an atomic image was a controversial topic when I first began to learn EM in 1973. We, therefore, attempted to confirm that an atomic image could be obtained without ambiguity. For an imaging sample, we used crystals of organic compounds, although many electron microscopists used inorganic crystals and/or dried droplets of heavy atom solutions, presumably because these samples are much easier to prepare and observe under an EM than organic chemicals. After many trials, we were able to observe an image of chlorinated copper phthalocyanine in which the copper atoms, porphyrin rings and chlorine atoms could be clearly discriminated (Fig. 2a) [5]. Although this image proved that EM could provide an atomic image, an extremely large number of images was required to obtain one high-quality (Scherzer's) focused image. Defocused images enhanced different image features, as shown in Fig. 2b. Nevertheless, because of radiation damage, the focus needed to be adjusted with a very dark electron beam by which one could not get the best focus condition (the Scherzer's focus image).

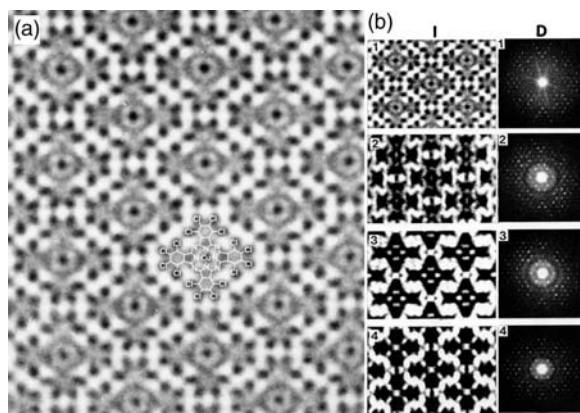


Fig. 2. High-resolution image of chlorinated copper phthalocyanine resolved at the atomic level by EM (a). Images under different defocus conditions (b). 1, 2, 3 and 4 indicate images under the Scherzer's focus condition 1000 Å underfocus, 1500 Å underfocus and 2000 Å underfocus, respectively.

To overcome this difficulty, we developed a system for focusing without the extra beam on the imaging specimen area and named the system the minimum dose system (MDS). High-resolution images of radiation-sensitive organic molecules, such as the silver-7,7',8,8'-tetracyanoquinonodimethane complex (Ag-TCNQ), were easily and reproducibly observed using the MDS (Fig. 3) [6]. Unlike organic molecules, biological molecules are extremely sensitive to radiation and the resolution of their images is therefore strongly restricted by radiation damage.

Radiation damage of biological molecules

The radiation and dehydration sensitivities of biological molecules were difficult obstacles that forced us to develop an effective and stable cryo-EM with a helium-cooled specimen stage and a cryo-transfer system for ice-embedded samples.

The electron beam inevitably broke chemical bonds of organic and biological materials. The produced radicals would then attack the circumference bonds, and molecular fragments would diffuse away. These events lead to the collapse of the initial structure. Radiation damage could effectively be reduced by minimizing the movements of the molecular fragments. Minimization of the movement of atoms and fragments also increases the population of reforming bonds. After many attempts to solve this radiation damage problem, only cooling of the biological specimen was found to reduce

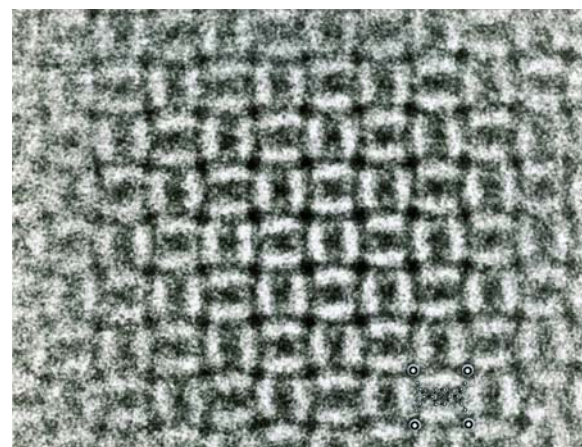


Fig. 3. High-resolution images of the silver-7,7',8,8'-tetracyanoquinonodimethane complex, Ag-TCNQ taken by MDS.

damage by limiting the movement of the atoms and molecular fragments.

Cooling the specimen to below 20 and 8 K reduced irradiation damage to the crystals of biological molecules compared with that induced at room temperature to $\sim 1/10$ and $1/20$, respectively [7]. The lattice heat capacity of all materials, however, becomes small at very low temperatures, such as the temperature of liquid helium. The heat conductivity of non-metals is also dramatically reduced at such a low temperature. Therefore, the temperature of the specimen could rise rapidly in the area being irradiated by an electron beam, which tends to change the thermal energy by interacting with the specimen. To confirm the actual temperature at the irradiated site, we developed an instrument to introduce gases, such as N_2 and Ne, which allowed us to estimate the specimen temperature by recording the electron diffraction patterns of solid N_2 and Ne. This indicated that the specimen temperature must have been lower than 20 K (N_2) and 8 K (Ne), even under the conditions used to record the electron diffraction patterns by which we measured the radiation damage of crystals of biological molecules.

Based on these observations, we attempted to develop a cryo-EM equipped with a specimen stage cooled by liquid helium. The boiling of the coolants, liquid N_2 and liquid He, however, caused mechanical vibrations. The specimen drift induced by temperature changes in the specimen stage was also difficult to control. These problems had to be overcome in the design of the high-resolution cryo-EM. The dehydration problem was overcome using the ice-embedding method of the rapid-freezing technique [8]. To effectively transfer an ice-embedded sample to the cryo-stage of the EM, however, a cryo-transfer system had to be developed.

Originally developed cryo-EM with a helium stage

For high-resolution data collection, two-dimensional (2D) crystals are embedded in a thin layer of an amorphous ice and/or a sugar solution, for which trehalose is recommended [9]. The specimen is then mounted on the cryo-stage of an EM using a cryo-transfer device. In this case, the thickness of the ice layer must be optimized for high-resolution data

collection because the flatness of 2D crystals is crucially important, especially for data collection with the specimen tilted relative to the electron beam. To minimize noise and to make the crystal flat, a thin layer of ice is better, but, in contrast, a thin ice layer dehydrates the sample. Observation of diffraction spots of 2D crystals, especially at resolutions higher than 3 Å, requires the best specimen preparation conditions. The best conditions are achieved only empirically, that is, by trial and error, because states of samples, such as crystal density and temperature, as well as humidity of the specimen preparation room, influence the thickness of the water layer on the specimen grid. Specimen preparation for cryo-EM therefore requires many trials to determine the very best specimen conditions for high-resolution data collection. To examine many specimen preparation conditions, the cryo-EM must be equipped with a quick specimen exchange device and a stable specimen stage. Therefore, we developed a cryo-EM with a stable helium stage as well as an effective cryo-transfer system by which we could exchange samples and obtain an image of the new sample at 2 Å resolution within 10 min. Figure 4 shows an electron diffraction pattern obtained at a resolution higher than 2 Å, which required many trials to optimize the specimen preparation conditions of the 2D crystals.

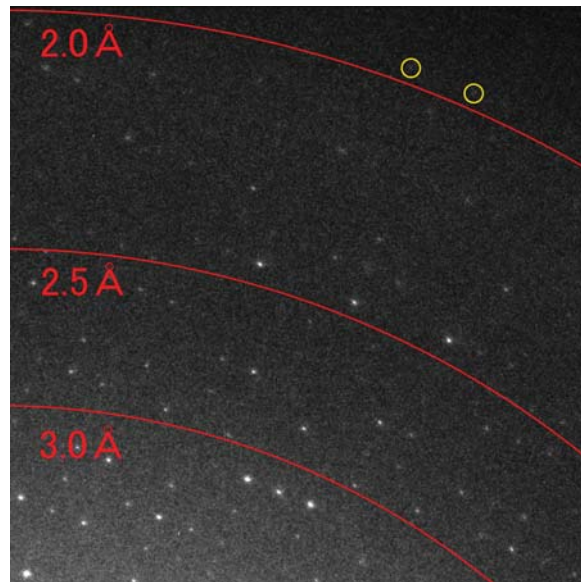


Fig. 4. High-resolution diffraction pattern of AQP4 in which spots were observed with resolution higher than 2 Å.

The resolution of an image of a biological macromolecule is usually limited to much less than 3 Å due to radiation damage. An atomic model can be made, however, if we can achieve 3D structure analysis at resolutions higher than 3 Å. In 1991, we developed a superfluid helium stage that allowed us to achieve a resolution of 2.6 Å [10]. The thermal shield of the liquid nitrogen and helium tank is gold-plated in order to minimize radial heat. A small liquid helium container, which is set at the center of the stage, is connected to the helium tank by a capillary and named the pot (Fig. 5a). The specimen in the pot is cooled down to 1.5 K using superfluid helium and we call this the 1.5 K pot, while we usually use the pot temperature at 4.2 K. Although the target resolution of our electron micrographs is something like 3 Å, an instrument yielding better resolution would be highly beneficial, because

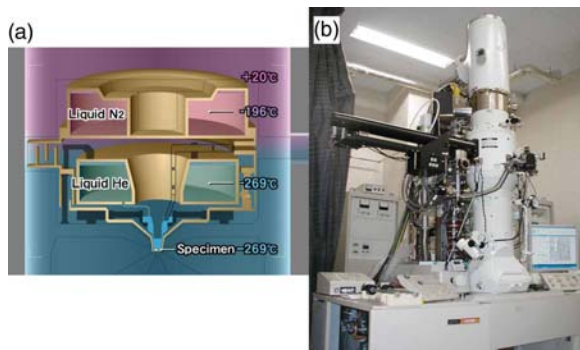


Fig. 5. Schematic figure of the original helium stage (a). Seventh-generation cryo-EM with outer control tilting system (b).

biological molecules comprise mainly light atoms that exhibit small atomic scattering factors in a high-resolution range. A higher resolution close to 2.5 Å might be required to identify water molecules. Based on the second-generation cryo-EM, we improved the resolution as well as operation of the cryo-EM with a top-entry-type helium stage. We then improved the instrumental resolution to 2.0 Å and overcame the operational difficulties [7]. The third-generation cryo-EM was a mature instrument for electron crystallography with a very stable cryo-stage. This cryo-EM included an effective cryo-transfer system and an automated, user-friendly system for ice-embedded specimens. The fourth-generation cryo-EM was equipped with an automatic cryo-transfer system. The fifth-generation cryo-EM was developed for mainly the single-particle method. Recently, we improved the sixth-generation cryo-EM, which is equipped with an outer-control tilting device, but not a eucentric system, to create the seventh-generation cryo-EM with a eucentric outer-control tilting device, for electron tomography and some other analyses (Fig. 5b).

Charge status analysis of bacteriorhodopsin

We analyzed the structure of bacteriorhodopsin together with lipid molecules using electron crystallography, as shown in Fig. 6a [11]. Atomic scattering factors for electrons are strongly affected by the

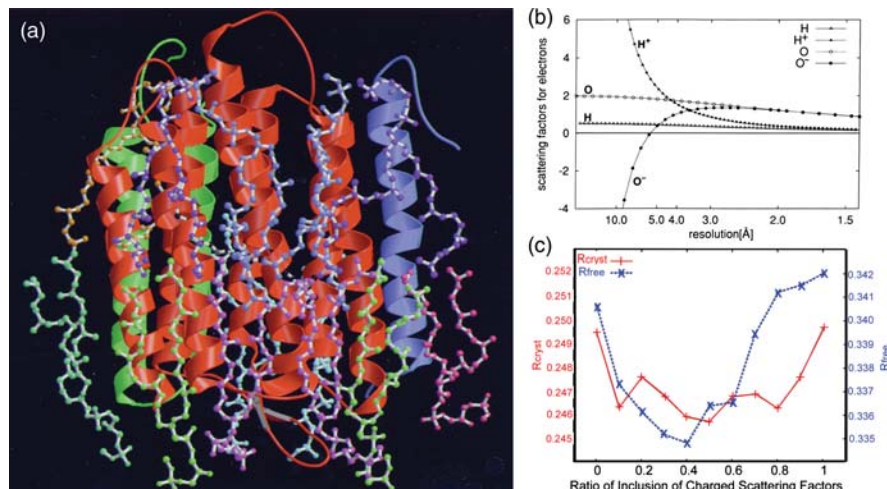


Fig. 6. Structure of bacteriorhodopsin together with lipid molecules (a). Atomic scattering factors of electrons for neutral and charged atoms (b). Comparison of refined results using various ratios of atomic scattering factors for neutral and charged atoms. R-factors (red) and free R-factors (blue) calculated using scattering factors of partially charged atoms for carbon and oxygen atoms in the peptide group. The minimum value for the R-factor and the free R-factor were observed at the charged ratios of 0.45 and 0.40, respectively (c).

charge status of atoms, unlike X-rays. Atomic scattering factors of neutral and charged atoms for electrons show largely different values, especially below 4.5 Å resolution (Fig. 6b). Although a neutral hydrogen atom has a small scattering factor, a positively charged hydrogen atom, proton, has a larger scattering factor than that of neutral oxygen. Comparison of refined results using various ratios of atomic scattering factors for neutral and charged atoms enabled us to examine the charge status of polypeptide carbonyl groups. R-factors (red) and free R-factors (blue) were calculated in refinements using scattering factors of partially charged atoms for carbon and oxygen atoms in the peptide groups of bacteriorhodopsin. The minimum values for the R-factor and the free R-factor were at the charged ration of 0.45 and 0.40, respectively (Fig. 6c). The results suggest that the negative charge of polypeptide carbonyl groups shifts to the oxygen atom from the carbon atom by about 40% on average [11]. When high-resolution structure analysis is achieved, careful analyses of the $|F_O| - |F_C|$ map with and without low-resolution data may provide information about the charge status of atoms based on electron crystallography.

When we attempted a structure analysis of bacteriorhodopsin, we encountered serious difficulties due to an image shift induced in the specimen due to charging, especially under tilted specimen conditions. We then acquired more than 10 000 images to obtain only about 200 good images, which was terribly tedious and inefficient. This was a serious problem for image data collection from 2D crystals. The image shift extinguishes optical diffraction spots perpendicular to the tilt axis, even in a medium- or low-resolution area. Almost all of the images from a tilted specimen prepared on a one-layer carbon support tend to be deteriorated by the image shift caused by beam-induced charging of the specimen. The success ratio for obtaining high-resolution images from tilted specimens is therefore only about 2%. To overcome this serious problem, we investigated the carbon sandwich preparation method, in which crystals are placed between two sheets of carbon film. When we used carbon-sandwiched specimens, the ratio of images showing deterioration in diffraction patterns due to an image shift was significantly decreased and the success

ratio improved to better than 90%. Thus, the carbon sandwich preparation method was confirmed to overcome the difficult problem and to contribute to more efficient structural analysis using electron crystallography [12].

Another advantage of the carbon sandwich technique was observed for the water channel aquaporin 0 (AQP0), where the dehydration problem was minimized and the structure could be analyzed at 1.9 Å [13]. At such a high resolution, lipid molecules together with water molecules in the AQP0 crystal are clearly discriminated.

Structure analyses of water channels

Water is the most abundant molecule in biological cells. Most cell membranes therefore require an effective water channel function. The cell membrane exquisitely regulates the entry and exit of ions because the ion concentration and its change are strongly related to cell signaling. The water channels (AQPs), therefore, need to maintain ionic conditions both inside and outside a cell, even while translocating a large amount of water. The regulation of pH in the cell is crucially important for cell functions, such as signal transduction, and cell proliferation and survival. An atomic model of AQP1 at 3.8 Å resolution produced by EM revealed the molecular basis of water selectivity while maintaining fast water transport [14]. This was also the first atomic-resolution structure of a human membrane protein. To accomplish the water channel functions effectively, the structure has a peculiar conformation, which we named the AQP fold (Fig. 7a).

The critical characteristic of AQP1 is its high water permeability, ~3 billion water molecules per channel per second. Almost all residues within a central 20 Å zone in the pore are highly hydrophobic, although those of a water channel had thought to be hydrophilic. A narrow part of the pore, ~3 Å in diameter, is located at the middle of the membrane, where loops B and E interact with each other, especially with proline 77 and 193 (AQP1) of the conserved Asn-Pro-Ala (NPA) sequences in all water channels. In addition to the enormous capacity for water conductance, the AQP1 pore also exhibits marked selectivity. Based

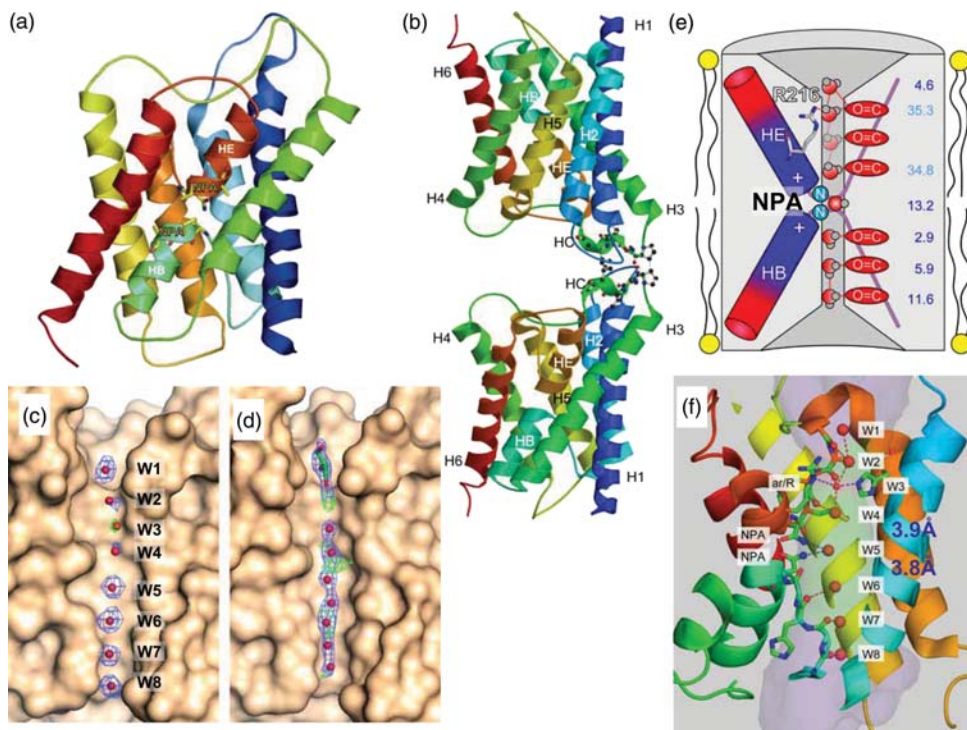


Fig. 7. Structure of AQP1 (a). Adhesive structure of AQP4 (b). Densities of water molecules in water channel of AQP4 analyzed by electron crystallography (c). Densities of water molecules in water channel of AQP4 analyzed by X-ray crystallography (d). Schematic figures of AQP4 structure and temperature factors of water molecules in the channel (e). Structure of AQP4 with water molecules analyzed by electron crystallography (f).

on structure analysis by electron crystallography, we proposed a model explaining the water selective mechanism that also maintains the high-speed water transport. This model is named the hydrogen bond isolation mechanism [14].

Another water channel, AQP4, is the predominant water channel in the mammalian brain and is therefore of great interest. We determined the AQP4 structure by electron crystallography of double-layered, 2D crystals that were prepared from AQP4 molecules expressed in Sf9 cells and purified using a detergent, *n*-octyl- β -D-glucopyranoside. Analysis of the AQP4 structure was complicated by variations in the double-layered 2D crystals in the lateral alignment and distance between the two layers [15]. Electron diffraction data were not sufficiently sensitive to select one specific crystal type among the crystal variants, despite the high resolution of 3.2 Å. Phase data extracted from the images at a medium resolution, on the other hand, were sensitive enough to discriminate between crystals with different arrangements of the two layers. The use of a helium-cooled EM [10] and the

carbon sandwich specimen preparation technique, which significantly increases the yield of good images [12], allowed us to also acquire an image of each crystal that produced a high-resolution diffraction pattern. Classification based on the image data, which provided phase information to better than 6 Å, identified one predominant crystal type that accounted for ~70% of the analyzed crystals yielding high-quality electron diffraction patterns. In this crystal type, the two layers have a spacing of 45 Å from molecule center to molecule center. The final 3.2 Å resolution intensity data set was used to determine the AQP4 structure by molecular replacement using the AQP1 structure. The images, which were recorded after the corresponding electron diffraction patterns and used for classification, were used to calculate a density map and confirmed the consistency of our structure [15].

Glial cells contain characteristic orthogonal arrays in the plasma membrane, which are especially prominent in glial end feet surrounding vascular capillaries in the brain. Immunogold labeling experiments showed that these arrays contain

AQP4 [16]. While both AQP4 and AQP1 function as very fast water-selective pores, AQP4 has distinctive biological characteristics as it forms orthogonal arrays in intact membranes. Furthermore, AQP4 exists in glial cells as a full-length protein starting with Met1 (AQP4M1) and an alternative shorter splicing isoform that starts with Met23 (AQP4M23). The freeze-fracture replica labeling technique allows us to examine how the expression of the long AQP4 splicing variant inhibits the orthogonal array formation of the short splicing variant [17].

AQP4 is also expressed in glial lamellae of the hypothalamus, where it may have a role in osmo-, thermo- and glucose-sensing. In glial lamellae, the plasma membrane forms large junctions between individual layers, which contain AQP4. Interestingly, another water channel, lens-specific AQP0, forms the ‘thin junctions’ between fiber cells. Structure analysis of AQP4 by double-layered 2D crystals revealed that the molecule contains a short β_{10} helix in an extracellular loop that mediates weak but specific interactions between AQP4 molecules in the adjoining membrane [15]. This finding suggests a previously unexpected role for AQP4 in cell adhesion (Fig. 7b). This notion was corroborated by the expression of AQP4 in L-cells, which resulted in the cells forming clusters. Our AQP4 structure thus enables us to propose models for the size regulation of orthogonal arrays and channel-mediated cell adhesion observed in the glial lamellae of the hypothalamus. AQP4 membrane junctions may reduce the water permeability of glial cell plasma membranes, because the tight tongue-in-groove packing of the two crystalline layers results in a partial blockage of the extracellular pore entrances. While packing of the AQP4 tetramers in the junctions must create resistance for water flowing across the two membranes, rapid water flow through the channels may also reduce the adhesion between the adjoining membranes. This may establish the basis for a role of AQP4 in osmo-sensing. For example, a high AQP4M1/AQP4M23 expression ratio produces small AQP4 arrays that provide weak adhesion between membranes, which could easily be separated and thus react to small water flows resulting from small osmotic differences. A low AQP4M1/AQP4M23 expression ratio, on the other hand, would result in extensive AQP4 arrays providing relatively strong

adhesion between membranes that would withstand large water flows associated with large osmotic differences. Although further experiments are required to elucidate the interplay of the two functions in AQPs and potentially other membrane channels with adhesive properties, we propose the name ‘adhennels’ for ‘adhesive water and ion channels’ [15].

Based on the electron crystallographic structure of AQP1, the hydrogen bond isolation mechanism was proposed to explain how AQPs are impermeable to protons despite their very fast water conduction. The mechanism by which AQPs exclude protons, however, is controversial. Therefore, we present the structure of AQP4 by electron crystallography of double-layered 2D crystals at a resolution of 2.8 Å. The improvement in data quality makes it possible to identify seven individual water molecules in the channel (Fig. 7c) [18]. In contrast, a map obtained using X-ray crystallography shows only blurred densities of water molecules in the channel, even at 1.8 Å resolution (Fig. 7d) [19]. In addition, the Fo–Fc map shows an additional spherical density at the ar/R constriction site (the green cage in Fig. 7c). Because the side chains of AQP4 around the ar/R region are represented by a clear density and the atoms of the protein molecule have low temperature factors in this region, we assigned an eighth water molecule to the spherical density at the ar/R site (Fig. 7c and W3, indicated as a weak density in Fig. 7e and smaller ball in Fig. 7f). The narrow diameter at this constriction would make it an unfavorable position for a water molecule, potentially explaining the weak density at this position. The two neighboring water molecules on either side of the ar/R constriction, which form hydrogen bonds with the unstable water molecule in the constriction, have higher temperature factors (35 \AA^2) compared with those of all the other water molecules in the channel ($2.9\text{--}13.2 \text{ \AA}^2$) (Fig. 7e).

In X-ray crystallography, a resolution of 2.8 Å would be considered too low to see water and lipid molecules, but our density map resolved all water molecules in the channel as well as lipid molecules. The B factors of the water molecules in the pore are lower than 40 \AA^2 (Fig. 7e), which is significantly lower than those of water molecules seen in membrane protein structures determined by X-ray

crystallography. To analyze the 3D structure of a membrane protein by electron crystallography, data must be collected from hundreds of 2D crystals. This has been considered as a disadvantage of electron crystallography, but our resultant density map clearly and counter-intuitively resolved eight spherical densities that could be assigned to water molecules (Fig. 7c). The perceived weakness of electron crystallography that data are collected from many different crystals may in fact be a strength of the technique. We collected more than a 1000 diffraction patterns, but selected only the 199 very best patterns [18] so that the final data set includes only information from the very best crystals. Furthermore, while we saw diffraction spots down to a resolution of 1.9 Å, we truncated the resolution of our density map to 2.8 Å. As a result of these procedures, the final lattice line data are of exceptionally high quality.

The small B factors of the water molecules might be due to the characteristic features of electron crystallography and/or the enhancement of the effect of the helical dipole moments due to the lipid environment. Using electron crystallography, lipid molecules were observed as schematically shown in Fig. 7e. In X-ray structures of AQPs in detergent micelles, the water molecules sometimes also display lower temperature factors compared with those of the surrounding main chain atoms, but the difference is usually less than 20 Å². Collecting the data at liquid helium temperature may account for our ability to observe water molecules in the AQP4 channel. We collected all the data for this structure analysis at a stage temperature of 4.2 K, and such a low temperature could clearly provide the lowest energy positions for water molecules in the channel.

The eight water molecules in the AQP4 channel are in a single-file arrangement as indicated by W1–W8 in Fig. 7f. From the measured distances between successive water molecules in the channel, all water molecules appear to form hydrogen bonds with the adjacent water molecule, as indicated by the red dotted lines in Fig. 7f, except for the water molecule at the NPA site and the one below it. These two water molecules (W5 and W6) thus seem to be separated from the other water molecules in the channel, lending support to the hydrogen bond

isolation mechanism. The inner surface of water channels is largely hydrophobic, except for the lining hydrophilic spots formed by the oxygen atoms of the main chain carbonyl groups of Gly209, Ala210, Ser211, His95, Gly94 and Gly93, and the nitrogen atoms of the side chain amide groups of Asn213 and Asn97 of the NPA motifs [18]. The line of mechanically stable carbonyl groups provides ‘a guide rail’ of hydrogen bonding partners for the hydrogen atoms of the permeating water molecules (Fig. 7e). Each water molecule in the single file can thus form two or three hydrogen bonds. Because water in bulk solution usually forms three or four hydrogen bonds with adjacent water molecules, water molecules entering the channel only have to sacrifice a single hydrogen bond, an energy cost of about 3 kcal. The arrangement of carbonyl and amide groups in the AQP4 channel thus dramatically lowers the energy barrier for water molecules entering the narrow AQP channel and allows for very fast water permeation through the otherwise hydrophobic channel.

The NPA motifs and the arrangement of the carbonyl groups in the hydrophobic channel together with the arrangement of the two short-pore helices HB and HE are crucially important to break the hydrogen bond network, which prevents proton conduction while maintaining fast water permeation. The ar/R constriction site might be important for blocking H₃O⁺, but not for the separation of hydrogen bonds. The higher-resolution structure of our AQP4 model supports the hydrogen bond isolation mechanism, which was previously proposed based on a lower-resolution structure of AQP1 [14] to explain the puzzling mechanism by which water channels can conduct water at very high speed while completely blocking proton permeation.

Gap junction channel

Connexion molecules form tight cell adhesive channels in the gap junction. Gap junctions contain intercellular communication channels that allow for the transfer of a wide variety of solutes of different sizes between the cytoplasm of adjacent cells. These solutes include ions, metabolites, nucleotides, peptides and secondary messengers. Gap

junction channels have critical roles in many biologically important processes, including cardiac development, fertility, the immune system and electrical signaling in the nervous system. The diversely expressed connexin26 (Cx26) is the second smallest member of the conserved mammalian gap junction protein family.

We focused on the structure of Cx26 gap junction channels and first used a site-specific human mutant Met34, hCx26M34A, because this mutant is expressed in baculovirus-infected Sf9 cells at higher quantities than are wild-type Cx26-infected cells. The hCx26M34A mutant is a single-site mutation at the same position as the hCx26M34T mutant, which can cause prelingual non-syndromic hereditary deafness [20]. Although the purified hemichannel is hexameric, the 2D arrays obtained by dialysis show an orthorhombic crystal lattice. The 3D map of the hCx26M34A mutant at 10 Å resolution reveals that the crystals are ~240 Å thick and contain three lipid bilayers. The 3D map also shows a novel density, which we named 'plug', in the center of the pore [21]. The dramatically reduced density in the structure of the N-terminal deletion mutant confirmed that the plug is formed by the N-terminal helices of six subunits in the hemichannel. The plug is located inside the membrane layer and forms contacts with the surrounding channel wall, which, at the constricted part of the vestibule, is formed by the innermost helices 1. This density strongly suggests that the plug physically blocks the channel within the membrane. Each hemichannel has its own plug, conferring it the ability to gate its pore autonomously. It is possible that the transjunctional voltage sensor and the physical gate reside exclusively within a single hemichannel.

X-ray crystallographic structural analysis at a higher resolution of the open state [22] provides more structural detail and supports the plug gating mechanisms in these widely expressed channels. The X-ray structure of wild-type Cx26, however, does not explain the multiple gating mechanisms of gap junction channels, because the cytoplasmic side is very fragile and 3D crystals were formed by the intermolecular interaction at the cytoplasmic side (Fig. 8a). Therefore, in the X-ray structure, the temperature factors of the N-terminal and cytoplasmic loops are very high. On the other hand, in

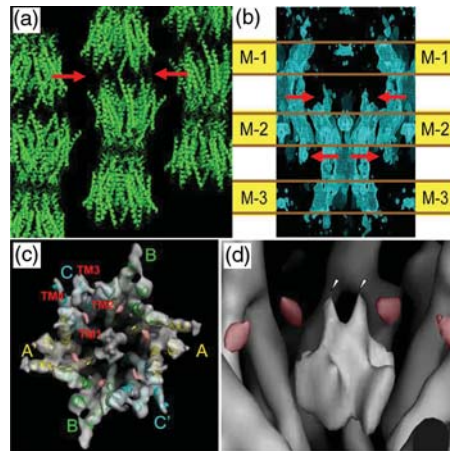


Fig. 8. Molecular packing in 3D crystals of gap junction channel (a). Molecular packing in 2D crystals, which is formed by three membrane layers (b). Gap junction structure with 2-fold symmetry (c) and two-layer arrangement of plug structure in the gap junction channel (d). Red densities could be related with loops between helix 1 to plug helix in each subunit.

2D crystals, the conformation of the cytoplasmic loop could be protected by two outer membrane layers, as shown in Fig. 8b. We were thus able to analyze the structure of this unstable channel by electron crystallography to evaluate the gating mechanisms from a structural point of view, including the interactions observed between adjacent subunits (Fig. 8c).

We recently improved the map of the hCx26M34A mutant based on electron crystallography. The analysis revealed that the plug-forming helices are not arranged with a 6-fold symmetry at a same height in the channel, but rather form a two-layer arrangement (Fig. 8c and d). The whole gap junction structure, especially the cytoplasmic parts, has a 2-fold, rather than 6-fold, symmetry (Fig. 8c). The cytoplasmic loop of the Cx26 molecule interacts with the plug loop and is therefore a key structural determinant for regulating the complex gating mechanism of gap junction channels [23].

Conclusions

The ability of electrons to form images, combined with advances in cryo-technology, enables the acquisition of detailed structural information about membrane proteins in their physiological lipid and ionic settings. This information complements that obtained by X-ray diffraction of proteins in detergent, in which the biological relevance of the

structure may be less certain. The development of cryo-electron tomography and real-space averaging methods together with instrument development, such as the seventh-generation cryo-EM, will extend the possibilities of obtaining high-resolution information from increasingly complex protein-lipid arrays and from living organisms.

Funding

This work was supported by grants-in-aid for Scientific Research (S) and the Japan New Energy and Industrial Technology Development Organization (NEDO).

Acknowledgements

This work performed in collaboration with many researchers whose names are recorded as authors in each referenced paper.

References

- 1 Sato C, Ueno Y, Asai K, Takahashi K, Sato M, Engel A, and Fujiyoshi Y (2001) The voltage-sensitive sodium channel is a bell-shaped molecule with several cavities. *Nature* **409**: 1047–1051.
- 2 Unwin N (1995) Acetylcholine receptor channel imaged in the open state. *Nature* **373**: 37–43.
- 3 Henderson R and Unwin P N (1975) Three-dimensional model of purple membrane obtained by electron microscopy. *Nature* **257**: 28–32.
- 4 Henderson R, Baldwin J M, Ceska T A, Zemlin F, Beckmann E, and Downing K H (1990) Model for the structure of bacteriorhodopsin based on high-resolution electron cryo-microscopy. *J. Mol. Biol.* **213**: 899–929.
- 5 Uyeda N, Kobayashi T, Ishizuka K, and Fujiyoshi Y (1979) High voltage electron microscopy for image discrimination of constituent atoms in crystals and molecules. *Chem. Scripta* **14**: 47–61.
- 6 Uyeda N, Kobayashi T, Ishizuka K, and Fujiyoshi Y (1980) Crystal structure of Ag-TCNQ. *Nature* **285**: 95–97.
- 7 Fujiyoshi Y (1998) The structural study of membrane proteins by electron crystallography. *Adv. Biophys.* **35**: 25–80.
- 8 Adrian M, Dubochet J, Lepault J, and McDowell A W (1984) Cryo-electron microscopy of viruses. *Nature* **308**: 32–36.
- 9 Hirai T, Murata K, Mitsuoka K, Kimura Y, and Fujiyoshi Y (1999) Trehalose embedding technique for high-resolution electron crystallography. *J. Electron Microsc.* **48**: 653–658.
- 10 Fujiyoshi Y, Mizusaki T, Morikawa K, Yamagishi H, Aoki Y, Kihara H, and Harada Y (1991) Development of a superfluid helium stage for high-resolution electron microscopy. *Ultramicroscopy* **38**: 241–251.
- 11 Kimura Y, Vassilyev D G, Miyazawa A, Kidera A, Matsushima M, Mitsuoka K, Murata K, Hirai T, and Fujiyoshi Y (1997) Surface of bacteriorhodopsin revealed by high-resolution electron crystallography. *Nature* **389**: 206–211.
- 12 Gyobu N, Tani K, Hiroaki Y, Kamegawa A, Mitsuoka K, and Fujiyoshi Y (2004) Improved specimen preparation for cryo-electron microscopy using a symmetric carbon sandwich technique. *J. Struct. Biol.* **146**: 325–333.
- 13 Gonon T, Cheng Y, Sliz P, Hiroaki Y, Fujiyoshi Y, Harrison S C, and Walz T (2005) Lipid–protein interactions in double-layered two-dimensional AQP0 crystals. *Nature* **438**: 633–638.
- 14 Murata K, Mitsuoka K, Hirai T, Walz T, Agre P, Heymann J B, Engel A, and Fujiyoshi Y (2000) Structural determinants of water permeation through aquaporin-1. *Nature* **407**: 599–605.
- 15 Hiroaki Y, Tani K, Kamegawa A, Gyobu N, Nishikawa K, Suzuki H, Walz T, Sasaki S, Mitsuoka K, Kimura K, Mizoguchi A, and Fujiyoshi Y (2006) Implications of the aquaporin-4 structure on array formation and cell adhesion. *J. Mol. Biol.* **355**: 628–639.
- 16 Rash J E, Yasumura T, Hudson C S, Agre P, and Nielsen S (1998) Direct immunogold labeling of aquaporin-4 in square arrays of astrocyte and ependymocyte plasma membranes in rat brain and spinal cord. *Proc. Natl. Acad. Sci. USA* **95**: 11981–11986.
- 17 Suzuki H, Nishikawa K, Hiroaki Y, and Fujiyoshi Y (2008) Formation of aquaporin-4 arrays is inhibited by palmitoylation of N-terminal cysteine residues. *Biochim. Biophys. Acta* **1778**: 1181–1189.
- 18 Tani K, Mitsuma T, Hiroaki Y, Kamegawa A, Nishikawa K, Tanimura Y, and Fujiyoshi Y (2009) Mechanism of aquaporin-4's fast and highly selective water conduction and proton exclusion. *J. Mol. Biol.* **389**: 694–706.
- 19 Ho J D, Yeh R, Sandstrom A, Chorny I, Harries W E C, Robbins R A, Miercke L J W, and Stroud R M (2009) Crystal structure of human aquaporin 4 at 1.8 Å and its mechanism of conductance. *Proc. Natl. Acad. Sci. USA* **106**: 7437–7442.
- 20 Kelsell D P, Dunlop J, Stevens H P, Lench N J, Liang J N, Parry G, and Leigh I M (1997) Connexin 26 mutations in hereditary non-syndromic sensorineural deafness. *Nature* **387**: 80–83.
- 21 Oshima A, Tani K, Hiroaki Y, Fujiyoshi Y, and Sosinsky G E (2007) Roles of Met-34, three-dimensional structure of a human connexin26 gap junction channel reveals a plug in the vestibule. *Proc. Natl. Acad. Sci. USA* **104**: 10034–10039.
- 22 Maeda S, Nakagawa S, Suga M, Yamashita E, Oshima A, Fujiyoshi Y, and Tsukihara T (2009) Structure of the connexin-26 gap junction channel at 3.5 Å resolution. *Nature* **458**: 597–602.
- 23 Oshima A, Tani K, Toloue M M, Hiroaki Y, Smock A, Inukai S, Cone A, Nicholson B J, Sosinsky G E, and Fujiyoshi Y (2011) Asymmetric configurations and N-terminal rearrangements in connexin26 gap junction channels. *J. Mol. Biol.* **405**: 724–735.